Journal of Modern Optics, 2013
Vol. 60, No. 14, 1136–1144, http://dx.doi.org/10.1080/09500340.2013.842614

Taylor & Francis
Taylor & Francis Group

Radiometric characterization of a novel LED array system for visual assessment

J.M.M. Linhares[a], H. Neves[b], D. Lopes-Ferreira[b], M. Faria-Ribeiro[b], S.C. Peixoto-de-Matos[b] and J.M. Gonzalez-Meijome[b]*

[a]*Faculty of Science and Technology, Anglia Ruskin University, East Road, Cambridge CB1 1PT, UK;* [b]*CEORLab - Centre of Physics, University of Minho, Campus de Gualtar, 4710-057, Braga, Portugal*

(*Received 4 April 2013; accepted 4 September 2013*)

Light that enters the eye can be distorted due to several factors leading to a poor visual performance. The purpose of this paper is to describe and characterize the light-emitting diode (LED) display system to be used in a new device to assess visual quality under high glare conditions. The device has a central white LED and surrounding white LEDs distributed in a radial manner. Each LED is controlled independently using special designed software. The spectral power distribution and color of the LEDs were assessed at different voltage intensities to test the response in terms of output luminance and spectral distribution. It was found that the typical maximum luminance was about 2800 cd/m^2 and 6 cd/m^2 for the central and surrounding LEDs, respectively. Their color was found to be within the ΔE^*_{ab} range of 2.6 and 0.23, respectively, if the minimum and maximum intensities are considered. The characterization of this device was proved successfully, which might indicate its usefulness in future visual assessments.

Keywords: night vision; visual assessment; haloes; glare; starburst

1. Introduction

Visual perception of fine details under dark backgrounds and in the presence of glare sources is a challenging task and its evaluation is of primary interest in activities such as driving at night, sailing, or piloting under night vision conditions [1]. Under such conditions, sources of light are surrounded by different features that impair the subject's ability to see the background, including haloes, glare, and starburst effects that had been proposed to be considered in conjunction under the term light distortions [2]. New modes of vision correction further challenge the visual system under dim light conditions. This is the case of multifocal optical devices to correct presbyopia [3] or surgical procedures of visual correction [4]. The advances in visual correction strategies have not been accompanied in certain aspects by sensitive methods to evaluate and quantify their consequences to the visual system and their impact on the quality of life of people undergoing such procedures.

Night vision disturbances have been a primary field of interest for clinicians and researchers [5,6]. Different devices have been developed to evaluate night vision under night conditions including some instruments [7] and psychometric tools [8]. Nevertheless, theoretical visual simulations continue to be the predominant way to approach a quantitative geometric description to help to understand the subjective perception of the patient [9]. However, these simulations consider almost exclusively the optical properties of the eye and might well ignore the neural part of the visual process. In fact, such simulations use to be based on the aberrations of the eye, and previous work has demonstrated that optical aberrations of the eye can only explain a small part of the variability in light distortion in patients undergoing corneal refractive surgery as measured with an experimental device [4]. Development of devices that can quantify and accurately describe the visual disturbances is desirable not only to quantify the consequences of different modes of vision correction and as a result of different ocular diseases, but also to quantify the improvements in result of different treatment strategies [10]. Some software-based devices to work on computer screens have been devised and applied clinically [11,12]. However these systems have several limitations, namely the intensity and contrast range achievable with such devices. It is not possible to simulate with bright spots on a screen certain effects that are still visible with real sources of light such as lines arising out from the source (starburst effect). Furthermore, the characteristics of the stimulus presented on CRT or TFT screens might be less reproducible between devices depending heavily on the individual screen configuration, thus affecting the inter-laboratory

*Corresponding author. Email: jgmeijome@fisica.uminho.pt
Disclosure: J.M. González-Méijome is co-inventor of the device whose characterization is presented here.

repeatability of the technology. Nevertheless, the use of such devices should be supported by a complete knowledge of its radiometric and correspondent lightness and chromatic characteristics before the clinical use.

The goal of this work was to characterize the radiometric properties of a new LED-based software – hardware integrated device aimed to characterize and quantify night visual disturbances in human subjects.

2. Methods

The purpose of this device is to assess the influence of visual disturbances on a patient's vision, in particular in visual conditions where bright lights in dark surrounds induce visual impairment. To simulate such a visual condition a device was devised to create a halo or starburst effect using a central LED. Surrounding LEDs with power individually controlled were also used. By adjusting the power of the surrounding LEDs until they are noticed by the patient under examination, and by recording the used power, it is possible to assess the impairment created by the light of the central LED at different power intensities. No impairment would be represented by all surrounding LEDs being visible at their lowest intensity independently of the intensity of the central LED. Full impairment would be represented by all surrounding LEDs being invisible at their maximum intensity independently of the intensity of the central LED.

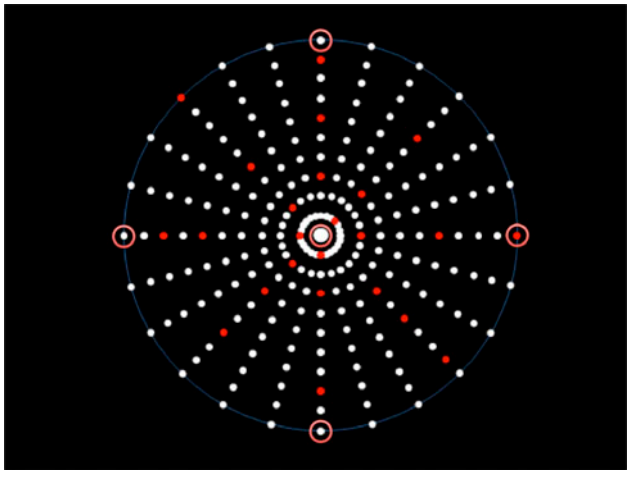

Figure 1. Layout of the LED array system for the visual assessment device. The central LED is a white LED from Agilent Technologies (HLMP-CW47-RU000). The surrounding white LEDs are from Avago Technologies (HSMW-CL25). Each one of the 24 lines of LEDs was separated by 15° and distributed radially; on each line the LEDs were separated by 5 mm. The LEDs indicated by red circles were those used in this study to characterize the surrounding LED array system. The LEDs represented in full red were used to randomly sample, with statistical significance, the entire array in terms of luminance. (The colour version of this figure is included in the online version of the journal.)

2.1. Description of the device

Figure 1 shows the layout arrangement of the central white light-emitting diode (LED) and the surrounding smaller white LEDs. The total size of the LED array system is 19 cm (W) × 22 cm (H). At the center there is the central white LED, which is larger and more powerful than the surrounding ones acting as a source of glare to challenge the subject's visualization of the dark background where the small LEDs are to be illuminated. The surrounding LEDs are distributed radially with a separation of 5 mm in 24 radial arrays. Radial arrays of LEDs are distributed in 24 lines in 15° steps. The device comprises a total of 240 surrounding LEDs. The central LED is responsible for creating the glare condition, while the surrounding LEDs were used as threshold discriminators at different positions and angular distances of the visual field and at different luminous intensities.

2.1.1. Central white LED

The central LED was a commercially available white LED (HLMP-CW47-RU000 from Agilent Technologies, Inc., UK). Figure 2 shows with a dotted dark line the normalized spectral power distribution of the radiance of the LED at its maximum intensity. The normalization constant was 0.0751 $W\,m^{-2}\,sr^{-1}$. The LED had a circular shape with a diameter of 5 mm and a height of 8.71 mm. Its intensity dropped to 50% at a viewing angle of 50°. It was controlled by in-house written software

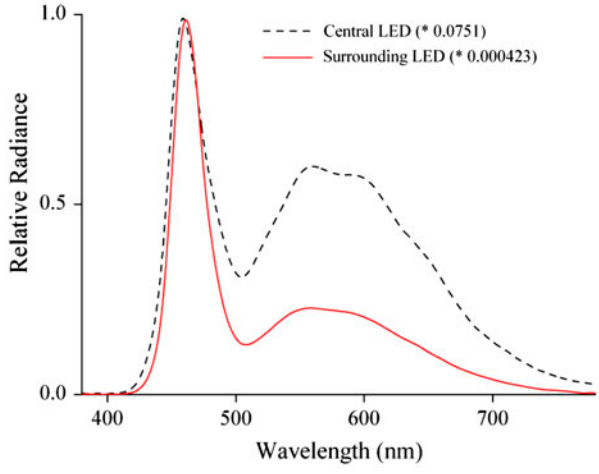

Figure 2. Normalized spectral power distribution of the central white and the typical surrounding white LEDs at maximum intensity. The curves represent an average of five measurements. The dark dotted line represents the central white LED. The red continuous line represents the surrounding LEDs. Also represented are the normalization constants. The standard deviation was also estimated but is too small to be seen in the given plot. (The colour version of this figure is included in the online version of the journal.)

capable of providing intensity variations in 0.1% steps through a user interface.

2.1.2. Surrounding LED

The surrounding LEDs were commercially available white LEDs (HSMW-CL25 from Avago Technologies, San Jose, CA). Figure 2 shows with a continuous red line the normalized spectral power distribution of the radiance of one of these LEDs at its maximum intensity. The normalization constant was $0.000423\,W\,m^{-2}\,sr^{-1}$. The LEDs had a rectangular shape of 1.6 (L) mm by 0.8 (W) mm and a height of 0.25 mm. Their intensity dropped to 50% at a viewing angle of 120°. It was controlled by an in-house written software capable of providing intensity variations in 1% steps through the user interface.

2.2. Radiometric measurements

The radiometric measurements were performed using a spectroradiometer with traceable calibration (SpectraColorimeter, PR-650, PhotoResearch Inc., Chatsworth, CA) positioned in the same location normally occupied by the patient. The distance between the spectroradiometer and the LED array was 2 m, the intended testing distance in the clinical setting.

2.2.1. Central LED

The central white LED was measured at different power intensities for both increasing and decreasing power intensities. Using the in-house built in controlling software, the power intensity was set to steps of 5% from 0% to 100% of the total available power in increasing and decreasing modes. At each power intensity, five radiometric measurements were taken and averaged. To assess the behavior of the central white LED on wider power adjustment steps, measurements were also taken on 20% steps at the same interval, but only in the increasing mode. All measurements were performed without a setup change with the spectroradiometer positioned perpendicular to the central LED.

2.2.2. Surrounding LEDs

The surrounding LEDs were measured at different increasing power intensities. Using the in-house built controlling software, the power intensity was set to steps of 15% from 0% to 100% of the total available power. At each power intensity, five radiometric measures were taken and averaged. All measurements were performed without a setup change. Initially the spectroradiometer was positioned perpendicular to the central LED and then oriented to the LED to be measured. This setup did not provide a perpendicular measurement position of the surrounding LEDs, but simulated the viewing conditions experienced by a real observer on an actual visual assessment session. The distance from the spectroradiometer to the LED array was kept constant at all times and invariant as different LEDs were measured. Only surrounding LEDs at extreme radial positions were assessed to provide the same measuring distance.

2.3. Colorimetric measurements

To assess eventual chromatic changes on the light emitted by the LEDs at different power intensities, the radiance data were converted into the CIE (x,y,Y) chromaticity coordinates assuming the standard CIE 1931 colorimetric observer [13]. They were then converted into the CIE 1976 uniform chromaticity scale diagram for better visualization [13]. The CIELAB coordinates [13] were estimated for each LED assuming as the reference illuminant the emitted spectral power distribution at maximum intensity. The CIELAB color differences between lower and higher power intensities were then estimated for each individual LED.

3. Results

Figure 3 shows the radiance measurements of the central white LED from 0% to 100% in increments of 10% of the total available power. Each curve represents an average of five measurements per intensity with the standard deviation being too small to be seen. Only steps of 10%

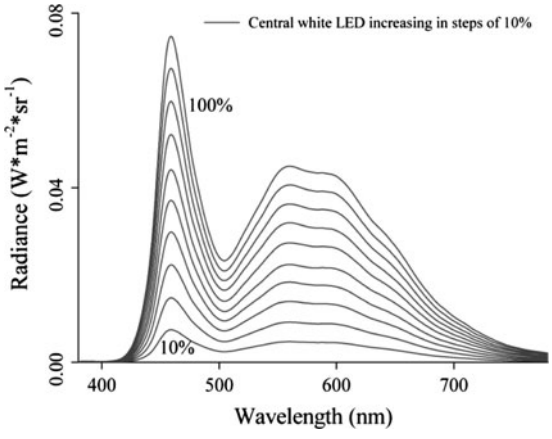

Figure 3. Spectral power distribution of the central white LED. Data were acquired from the lowest to the maximum power intensity in steps of 10% increments. Each curve represents an average of five measurements at each power intensity. The standard deviation was also estimated but is too small to be seen in the given plot.

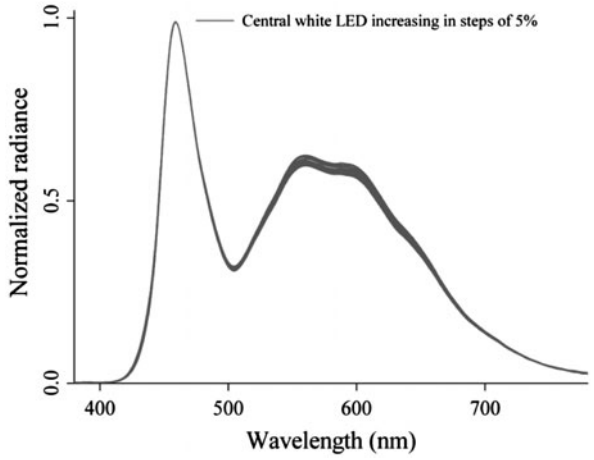

Figure 4. Normalized spectral power distribution of the central white LED. Data were acquired from the lowest to the maximum power intensity in steps of 10% increments and then normalized. Each of the 10 normalized curves presented represents an average of five measurements at each power intensity. The standard deviation was also estimated but is too small to be seen in the given plot.

are represented here for better clarity. The overall data were estimated in steps of 5% of the total available power. Figure 4 presents the same set of data as in Figure 3 but with normalized data to compare the spectral curves discarding the information of the radiance intensity. On this figure, all available data are

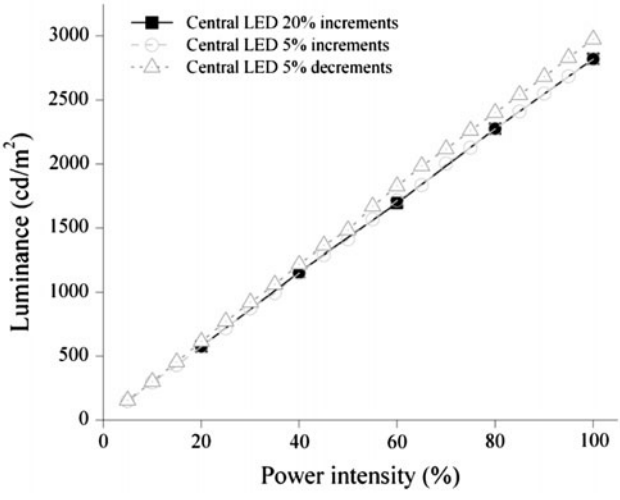

Figure 5. Luminance of the central white LED at different power intensities. Circles represent 5% increments in the power intensity, from 0% to 100%. Triangles represent 5% decrements in the power intensity, from 100% to 0%. Squares represent 20% increments in the power intensity, from 0% to 100%. Data were estimated as an average of five measurements at each power intensity. The standard deviation was also estimated but is too small to be seen in the given plot. The CIE 1931 colorimetric observer [13] was assumed when estimating the luminance from the radiometric data.

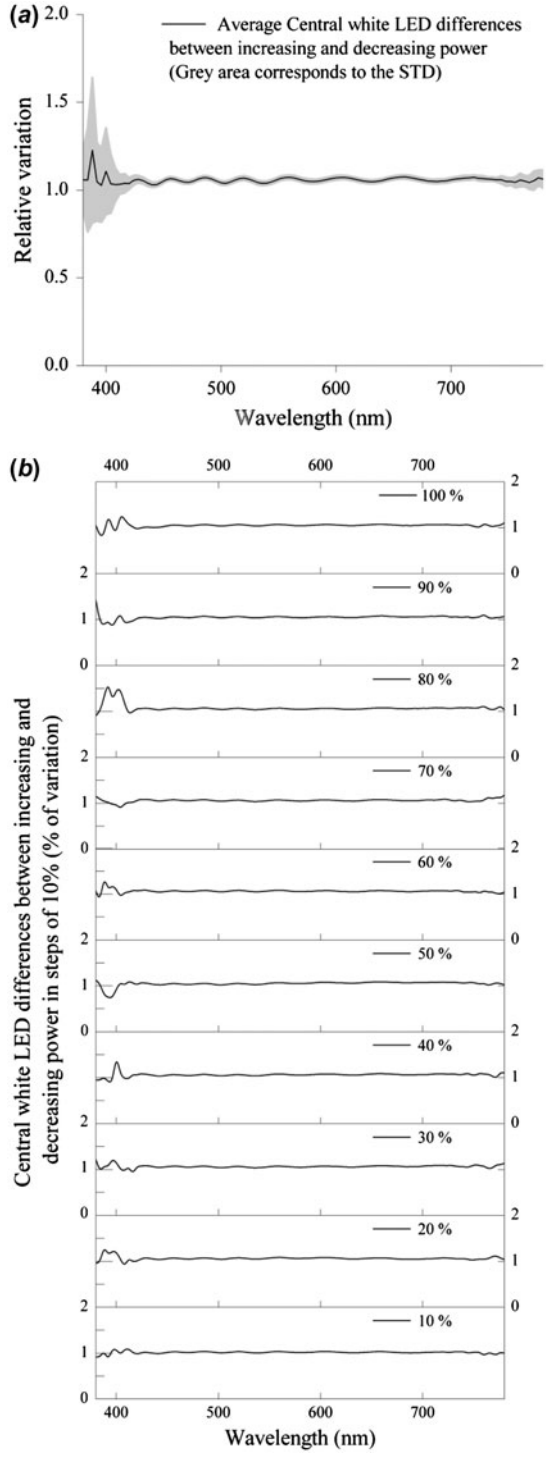

Figure 6. Variations on the radiometric spectrum between increasing and decreasing the power intensity of the central white LED at 5% steps. (*a*) Continuous dark line represents the average of the data across the different power intensities. Grey area represents the correspondent standard deviation at each wavelength. A variation of 0.5 on the given scales represents a variation of 50% in total. The average of the variations across wavelengths is around 6% with a STD of 2%. (*b*) Continuous dark lines represent the differences per wavelength at power intensities steps of 10%. A variation of 0.5 on the given scales represents a variation of 50% in total.

Table 1. Average and standard deviation of the variation on the radiometric spectra between increasing and decreasing the power intensities of the central white LED from 0% to 100% in 5% steps (same data as in Figure 6). As an example, variation of 1.10 represents an average variation of 10% from one measure to the other across intensities. The overall average of the total differences is of about 6% with a STD of about 2%.

Wavelength (nm)	Average	STD	Wavelength (nm)	Average	STD	Wavelength (nm)	Average	STD
380	1.10	0.17	516	1.10	0.01	652	1.10	0.01
384	1.10	0.29	520	1.10	0.01	656	1.10	0.01
388	1.20	0.41	524	1.10	0.01	660	1.10	0.01
392	1.00	0.22	528	1.10	0.01	664	1.10	0.01
396	1.00	0.21	532	1.00	0.01	668	1.10	0.01
400	1.10	0.25	536	1.00	0.01	672	1.10	0.01
404	1.00	0.17	540	1.00	0.01	676	1.10	0.01
408	1.00	0.09	544	1.00	0.01	680	1.10	0.01
412	1.00	0.06	548	1.10	0.01	684	1.10	0.01
416	1.00	0.05	552	1.10	0.01	688	1.00	0.01
420	1.00	0.03	556	1.10	0.01	692	1.10	0.01
424	1.10	0.03	560	1.10	0.01	696	1.10	0.01
428	1.10	0.02	564	1.10	0.01	700	1.10	0.01
432	1.10	0.02	568	1.10	0.01	704	1.10	0.01
436	1.00	0.02	572	1.10	0.01	708	1.10	0.01
440	1.00	0.01	576	1.10	0.01	712	1.10	0.01
444	1.00	0.01	580	1.00	0.01	716	1.10	0.01
448	1.00	0.01	584	1.10	0.01	720	1.10	0.01
452	1.10	0.01	588	1.10	0.01	724	1.10	0.01
456	1.10	0.01	592	1.10	0.01	728	1.10	0.02
460	1.10	0.01	596	1.10	0.01	732	1.10	0.01
464	1.10	0.01	600	1.10	0.01	736	1.10	0.01
468	1.00	0.01	604	1.10	0.01	740	1.10	0.01
472	1.00	0.01	608	1.10	0.01	744	1.10	0.02
476	1.10	0.01	612	1.10	0.01	748	1.00	0.03
480	1.10	0.01	616	1.10	0.01	752	1.00	0.02
484	1.10	0.01	620	1.10	0.01	756	1.00	0.03
488	1.10	0.01	624	1.10	0.01	760	1.10	0.04
492	1.10	0.01	628	1.00	0.01	764	1.10	0.03
496	1.10	0.01	632	1.00	0.01	768	1.00	0.04
500	1.00	0.01	636	1.10	0.01	772	1.10	0.05
504	1.00	0.01	640	1.10	0.01	776	1.10	0.04
508	1.00	0.01	644	1.10	0.01	780	1.10	0.05
512	1.10	0.01	648	1.10	0.01			

represented, from 0% to 100% in steps of 5% of the total available power.

Figure 5 shows the luminance of the central white LED estimated from the radiance data at several power intensities from 0% to 100% of the total available power. Increment steps of 5% are represented with circles; decrement steps of 5% are represented with triangles; increment steps of 20% are represented with squares. The luminance data was estimated from the radiometric data assuming the CIE 1931 colorimetric observer [13].

Figure 6 shows the variations in the spectral power distribution of the central white LED at different intensity powers. Spectral differences were estimated between the increasing and decreasing power intensities in 5% steps and taken at correspondent power intensities in each case. These differences were then averaged to produce the data represented as a black line and the STD as a gray area. A variation of 0.5 on the given scale represents a variation of 50% in total. The average of the variations across wavelengths is of about 6% with a STD of 2%. The majorities of the differences occur on the extremes of the wavelengths analyzed and correspond to very low light intensity with almost no impact on the visual perception. Table 1 presents the data used to create this figure.

Figure 7 shows the radiance measurements of one of the surrounding white LEDs from 0% to 100% in increments of 15% of the total available power. Each curve represents an average of five measurements per intensity with the standard deviation being too small to be seen. Figure 8 shows the same set of data as in Figure 7 but with normalized data to compare the spectral curves discarding the information of the radiance intensity. On this figure data was represented, from 0% to 100% in steps of 15% of the total available power.

Figure 9 shows the average of the luminance of four surrounding white LEDs at different power intensities

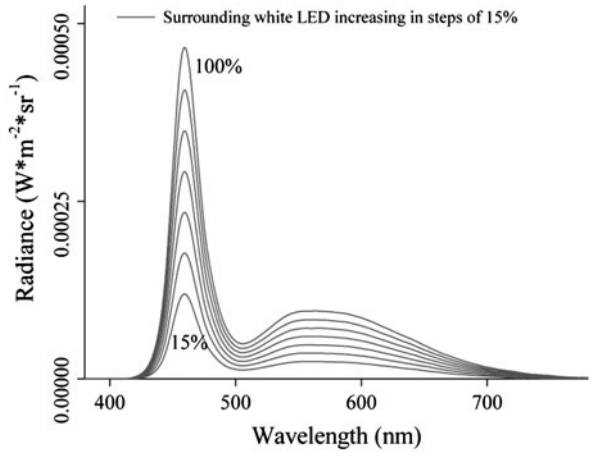

Figure 7. Spectral power distribution of one of the surrounding white LED. Data were acquired from the lowest to the maximum power intensity in steps of about 15% increments. Each curve represents an average of five measurements at each power intensity. The standard deviation was also estimated but is too small to be seen in the given plot.

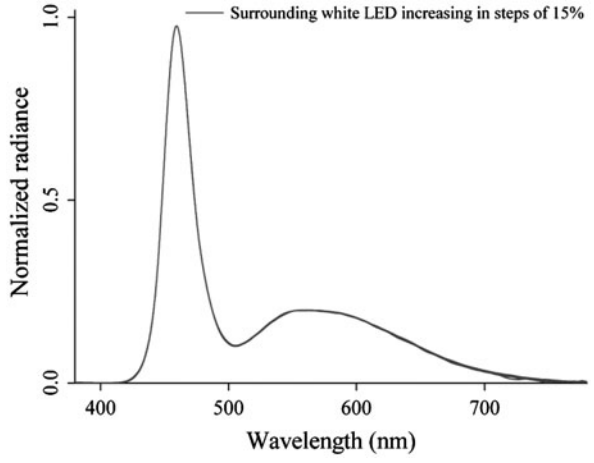

Figure 8. Normalized spectral power distribution of one of the surrounding white LEDs. Data were acquired from the lowest to the maximum power intensity in steps of about 15% increments and then normalized. Each one of the six normalized curves presented represents an average of five measurements at each power intensity. The standard deviation was also estimated but is too small to be seen in the given plot.

ranging from 0% to 100% of each individual LED maximum power intensity, as represented with red circles in Figure 1. The average was taken across five measurements per LED, for all LEDs, in intensity steps of 15% increments of the total available power. The accounted STD is represented with vertical error bars. The luminance data was estimated from the radiometric data assuming the CIE 1931 colorimetric observer [13].

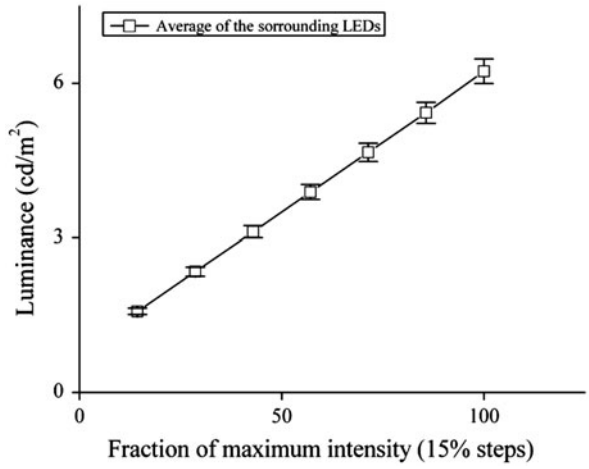

Figure 9. Average of the luminance of four surrounding white LEDs (as represented on Figure 1) at increasing power intensities. Open squares represent increments of about 15% of the total power intensity, from 0% to 100%. Data were estimated as an average of five measurements per power intensity for each LED. Vertical error bars represent the accounted standard deviation. The CIE 1931 colorimetric observer [13] was assumed when estimating the luminance from the radiometric data.

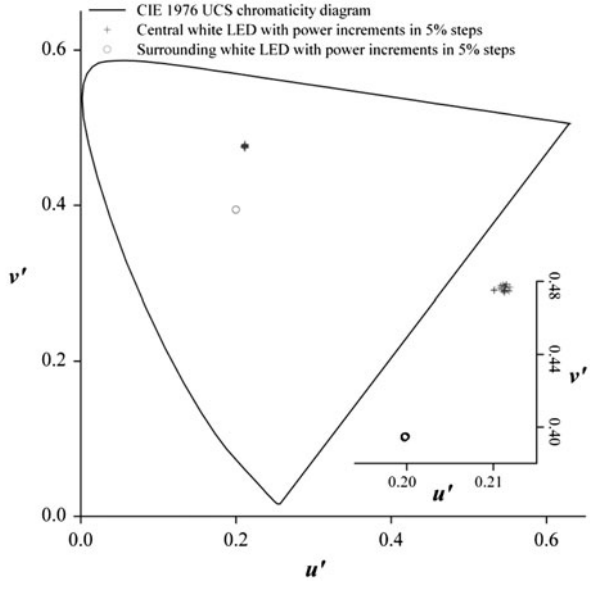

Figure 10. CIE 1976 UCS chromaticity diagram representing with plus signs the chromaticity coordinates of the central white LED at increasing intensities from 0% to 100% at 5% steps and with open circles the chromaticity coordinates of the horizontal left surrounding LED at increasing intensities from 0% to 100% at 15% steps. The inset presents the same data at a different scale for better visualization. Coordinates were estimated from the radiance data assuming the CIE 1931 colorimetric observer [13].

To better assess the impact on the spectral power distribution (and hence the impact on the color percep-

Table 2. Maximum CIE 1976 a,b (CIELAB) color differences, ΔE^*_{ab}, between different intensity power for the analyzed LEDs. All data were estimated assuming, as the reference white, each LED at maximum power and ignoring the luminance dimension.

LED	Max ΔE^*_{ab}	Average ΔE^*_{ab}
Central increasing	2.43	2.6
Central decreasing	2.81	
Surrounding up	0.26	0.23
Surrounding down	0.26	
Surrounding left	0.35	
Surrounding right	0.21	

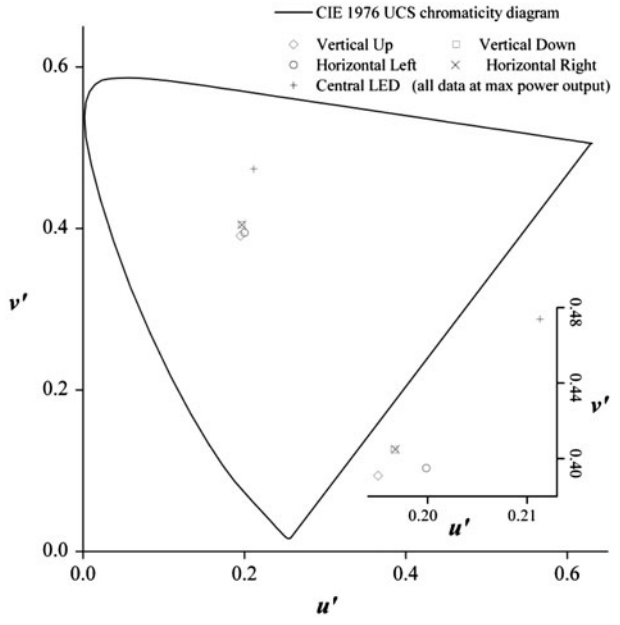

Figure 11. CIE 1976 UCS chromaticity diagram representing in open circles, crosses, open diamonds, and open squares the corresponding LEDs on the most extreme horizontal left arm, horizontal right arm, vertical superior arm, and vertical inferior arm, respectively, at maximum power intensities. The central white LED is represented by a plus sign at maximum power intensity. The inset presents the same data at a different scale for better visualization. Coordinates were estimated from the radiance data assuming the CIE 1931 colorimetric observer [13].

tion) of changing the power intensity of the LEDs their chromaticity coordinates on the CIE 1976 UCS chromaticity diagrams were estimated. Figure 10 represents with crosses and open circles the chromatic variations over power intensities changes for the central LED and one of the surrounding LEDs (the horizontal left LED), respectively. The central LED data was obtained in 5% steps and the surrounding LED data in steps of 15%. In both cases the power intensity interval was from 0% to 100%. The small inlet in the graph represents the same data as the bigger plot with a scale adjusted for better viewing. From there it is possible to see that the color of the central LED changes more than the surrounding LED.

As presented in Table 2, the maximum difference between the central LED at maximum power intensity and one of the other power intensities (in 5% steps) is of about 2.6 ΔE^*_{ab} in average (assuming the increments and decrements variations). All data were estimated assuming as the reference white each LED at maximum power and ignoring the luminance dimension. In general a just noticeable difference of around 1 ΔE^*_{ab} is assumed [14,15], but other authors will consider 2.3 ΔE^*_{ab} as the threshold value for surface colors [14,15]. The average ΔE^*_{ab} of the surrounding LEDs when comparing the LED output at maximum power intensity with other power intensities was of about 0.23, showing a smaller chromatic variation than the central white LED. Figure 11 represents the chromatic differences between the central LED and the four surrounding LEDs, all emitting at maximum power intensity.

4. Discussion

The purpose of this set of experiments was to characterize a new device intended to be used for the assessment of the impact of glare, haloes, and starburst (light distortions) in visual performance under night vision conditions. The device is composed of a central white LED with a high intensity power output and surrounding LEDs with smaller intensity power outputs. The clinical assessment will be performed by asking the patient to look at the central LED and assess the patient's discriminability of the surrounding LEDs at different intensity levels. The central LED is responsible for creating the glare condition while the surrounding LEDs are used as threshold discriminators at different positions and angular distances of the visual field. Similar approaches exist but are software based, where the glare source and peripheral detection stimuli are presented on a computer screen [12]. The LED array and central glare source characterized in this study are intended to work on a stand-alone platform full integrated with its own control software and user interface. This software will be mainly helpful in the definition and control of the eye examination routines and further extraction of results in a graphical layout. The device was characterized by measuring the luminance, the spectral power distribution, and the chromaticity of the central and surrounding LEDs. The central white LED was fully characterized at different increasing and decreasing power intensity steps. The surrounding LEDs were characterized by using four representative LEDs at peripheral extremes of the device assuming only increasing intensity levels in steps of about 15% increments. The chromatic differences

between maximum LED outputs and several lower power intensities are below the chromatic discrimination level on the surrounding LEDs and slightly above on the central white LED [14,15]. These results are unlikely to change the final outcome as at the stage of clinical assessment the central white LED will be kept constant while the variation intensity will be done on the surrounding LEDs.

The dependence of the surrounding LEDs on angular misalignments was also tested and found to be very dependent on proper alignment. Differences of about 50% in luminance intensity were found with very small tilts. It is thus paramount that proper alignment is achieved before any clinical trials. Non-diffused LEDs have been used to increase the LED output and the use of diffuse LEDs will certainly have an impact on the achievable final outcome, in particular on the final alignment of the setup. Nevertheless, the selected LEDs have a good angular emission for the intended usable distance (2 m from the source) and, since the relative output of the peripheral LED towards the central LED is more important than the absolute intensity on their own, the impact of the type of the LEDs selected should be minimal.

A statistical sampling of 10% the surrounding LEDs was performed and their luminance measured with a luminance meter (Konica Minolta, Inc. LS-110, Japan). The tested LEDs are the ones represented in full red on Figure 1. An average variation of 15% was found across the sample of the 24 LEDs. Despite this variation it is unlikely that this result will create a bias on the clinical test, as the intensity power of each surrounding LED can be independently adjusted to match the intended outcome.

The nature of the stimulus and the task involved has certain interactions with the visual system and its ability to discriminate a small stimulus against a dark background. The visual system is a dynamic system where the focus is changed to adjust the retinal image quality through the accommodation system. This system might respond quite randomly in the absence of stimulus, leading to the so-called empty space myopia or dark focus which is an error in the tonic accommodation status of the eye. Also, when the eye observes a small bright stimulus against a dark background, the accommodative status might change in order to adjust the visualization of the object under such conditions. It has been also demonstrated that this kind of visual task (which is a photopic condition instead of a scotopic condition as that leading to dark focus) can also lead to an over-accommodation and producing the so-called night myopia effect [16]. Thus, if the eye of non-presbyopic subjects is not under the effect of a cycloplegic drug, the visualization of the central and peripheral LED might be altered and changed over time during the course of an examination. However, this is the habitual condition experienced by subjects, so the present device might well reflect daily life tasks as seeing distant lights, stars, or car lights against a dark background under changing accommodation conditions.

One potential limitation of the device described is to maintain a constant intensity for all peripheral LEDs. It is known that the visual system is naturally apodized such that light entering at an angle through the pupil will have less impact due to the Stiles–Crawford effect [17]. Furthermore, the proximity of the inner peripheral LEDs to the central LED might involve summation and rivalry between the receptive fields for small stimulus [18] and change the overall perceptual signaling. Thus, it might be possible that equal intensity in the peripheral LED does not warrant equality in discriminative difficulties at different distances to the central LED. However, this might be easily compensated through the custom-made software able to control each one of the 240 peripheral LEDs separately.

The thermal stability of the LEDs may also influence their performance. In the particular case of this device and under clinical use, such a property is not expected to influence the final result as the power of the central LED will be kept constant and the surrounding LEDs will be adjusted independently, the important parameter being the relation between the central LED and the peripheral LED at the assessment time and not their individual intensities. As an example and considering the central LED at its maximum intensity, measurements taken over a time of about 2 min have variations smaller than 1 cd/m^2.

The stability of the luminance, chromaticity coordinates, and spectral power distribution of the LEDs over time cannot be estimated at the moment due to the novelty of the device, but further studies will be carried out to assess the impact of time on the output of the device.

Despite the limitations discussed here, the calibration and radiometric description of this novel LED array system for visual assessment was proved successful. The innovative software–hardware interface, which enables individual control of the intensity power of each one of the 240 surrounding LEDs and central white LED, is also of valuable use in the compensation of such limitations. Such results indicate the possibility of use of this LED array system for visual assessment in clinical environments in the near future.future.

Acknowledgements

This study has been funded by FEDER through the COMPTETE Program and by the Portuguese Foundation for Science and Technology (FCT) in the framework of projects PTDC/SAU-BEB/098391/2008, PTDC/SAU-BEB/098392/2008 and the Strategic Project PEST-C/FIS/UI607/2011.

References

[1] Cohen, Y.; Zadok, D.; Barkana, Y.; Shochat, Z.; Ashkenazi, I.; Avni, I.; Morad, Y. *Acta Ophthalmol. Scand.* **2007,** *85,* 367–370.

[2] Klyce, S.D. *Br. J. Ophthalmol.* **2007,** *91,* 992–993.

[3] Chu, B.S.; Wood, J.M.; Collins, M.J. *Invest. Ophthalmol. Visual Sci.* **2010,** *51,* 4861–4866.

[4] Villa, C.; Gutierrez, R.; Jimenez, J.R.; Gonzalez-Meijome, J.M. *Br. J. Ophthalmol.* **2007,** *91,* 1031–1037.

[5] Pop, M.; Payette, Y. *Ophthalmology* **2004,** *111,* 3–10.

[6] Fan-Paul, N.I.; Li, J.; Miller, J.S.; Florakis, G.J. *Surv. Ophthalmol.* **2002,** *47,* 533–546.

[7] Lackner, B.; Pieh, S.; Schmidinger, G.; Hanselmayer, G.; Simader, C.; Reitner, A.; Skorpik, C. *J. Cataract Refractive Surg.* **2003,** *29,* 444–450.

[8] McAlinden, C.; Pesudovs, K.; Moore, J.E. *Invest. Ophthalmol. Visual Sci.* **2010,** *51,* 5537–5545.

[9] Reinstein, D.Z.; Archer, T.J.; Gobbe, M. *J. Refractive Surg.* **2012,** *28,* 139–143.

[10] Villa-Collar, C.; Gonzalez-Meijome, J.M.; Gutierrez-Ortega, R. *J. Refractive Surg.* **2009,** *25,* 591–598.

[11] Gutierrez, R.; Jimenez, J.R.; Villa, C.; Valverde, J.A.; Anera, R.G. *J. Biomed. Opt.* **2003,** *8,* 663–667.

[12] Ortiz, C.; Castro, J.J.; Alarcon, A.; Soler, M.; Anera, R.G. *Appl. Ergon.* **2013,** *44,* 523–531.

[13] CIE. *Colorimetry*; CIE Publication 15:2004. CIE: Vienna, 2004.

[14] Pointer, M.R.; Attridge, G.G. *Color Res. Appl.* **1998,** *23,* 52–54.

[15] Mahy, M.; Van Eycken, L.; Oosterlinck, A. *Color Res. Appl.* **1994,** *19,* 105–121.

[16] Lopez-Gil, N.; Peixoto-de-Matos, S.C.; Thibos, L.N.; Gonzalez-Meijome, J.M. *J. Vision* **2012**, *12*, 1–9.

[17] Navarro, R.; Losada, M.A. *Optom. Vision Sci.* **1997,** *74,* 540–547.

[18] Redmond, T.; Zlatkova, M.B.; Vassilev, A.; Garway-Heath, D.F.; Anderson. R.S. *Optom. Vision Sci*. **2013**, *90*, 66–74.